

Kinematics of hypervelocity stars in the triaxial halo of the Milky Way

Qingjuan Yu^{*} and Piero Madau[†]

Department of Astronomy and Astrophysics, University of California, Santa Cruz, CA 95064
yyq@ucolick.org; pmadau@ucolick.org

7 November 2018

ABSTRACT

Hypervelocity stars (HVSs) ejected by the massive black hole at the Galactic center have unique kinematic properties compared to other halo stars. Their trajectories will deviate from being exactly radial because of the asymmetry of the Milky Way potential produced by the flattened disk and the triaxial dark matter halo, causing a change of angular momentum that can be much larger than the initial small value at injection. We study the kinematics of HVSs and propose an estimator of dark halo triaxiality that is determined only by instantaneous position and velocity vectors of HVSs at large Galactocentric distances ($r \gtrsim 50$ kpc). We show that, in the case of a substantially triaxial halo, the distribution of deflection angles (the angle between the stellar position and velocity vector) for HVSs on bound orbits is spread uniformly over the range 10° – 180° . Future astrometric and deep wide-field surveys should measure the positions and velocities of a significant number of HVSs, and provide useful constraints on the shape of the Galactic dark matter halo.

Key words: black hole physics – Galaxy: center – Galaxy: halo – stellar dynamics

1 INTRODUCTION

Recent observations have revealed the existence of a population of hypervelocity stars (HVSs) traveling in the halo of the Milky Way (MW) with Galactic rest-frame velocities v_{rf} in the range between $+400$ and $+750$ km s^{-1} (Brown et al. 2005; Edelmann et al. 2005; Hirsch et al. 2005; Brown et al. 2006a,b). HVSs are probably B-type main sequence stars with lifetimes $\lesssim 100$ Myr, Galactocentric distances > 50 kpc, and move with speeds large enough to escape from the Galaxy. The significant excess of B-type stars with velocities $+275 < v_{\text{rf}} < +450$ km s^{-1} and distances > 10 kpc observed by Brown et al. (2007) may also be an indication that many HVSs are ejected into the halo on *bound* orbits.

HVSs were first recognized by Hills (1988) as an unavoidable byproduct of the presence a massive black hole (BH) in the Galactic center. Only a close encounter with a relativistic potential well can accelerate a 3–4 M_\odot star to such extreme velocities, and at least three different ejection mechanisms have been proposed: the interaction between background stars and an intermediate-mass black hole (IMBH) inspiralling towards Sgr A*

(Yu & Tremaine 2003; Levin 2006; Baumgardt et al. 2006; Sesana et al. 2006), the disruption of stellar binaries in the tidal field of Sgr A* (Hills 1988; Yu & Tremaine 2003; Ginsburg & Loeb 2006; Bromley et al. 2006), and the scattering of stars off a cluster of stellar-mass BHs orbiting Sgr A* (O’Leary & Loeb 2006). In all these models, HVSs have unique kinematics compared to other halo stars: 1) they have almost zero initial specific angular momentum at ejection, $\sqrt{GM_{\text{BH}}r_p} \simeq 4.0 \times 10^{-6} \text{ kpc}^2 \text{ Myr}^{-1} (M_{\text{BH}}/3.6 \times 10^6 M_\odot)^{1/2} (r_p/10^{-6} \text{ kpc})^{1/2}$, where M_{BH} the mass of Sgr A* and r_p the pericenter distance of the star; 2) their high speeds diminish the impact of two-body relaxation or dynamical friction effects on their motion; and 3) their trajectories will deviate from being exactly radial because of the asymmetry of the Milky Way potential produced by the flattened disk and the triaxial dark matter (DM) halo, causing a change of angular momentum that can be much larger than the initial small value. (For reference, a 1 km s^{-1} deviation of the velocity from the radial direction at 50 kpc represents a change of $0.05 \text{ kpc}^2 \text{ Myr}^{-1}$ in specific angular momentum.) Proper-motion measurements of HVSs may therefore become a key diagnostic tool for constraining the shape of the Galactic potential (Gnedin et al. 2005).

Triaxial halos are a generic prediction of the hierarchical, cold dark matter (CDM) models of structure formation. Dissipationless cosmological simulations typically predict minor-to-major density axis ratios in the range 0.4–0.8

^{*} Also a Hubble Fellow at the Department of Astronomy, University of California at Berkeley, Berkeley, CA 94720.

[†] Also at the Max-Planck-Institut für Astrophysik, Karl-Schwarzschild-Str. 1, 85740 Garching, Germany.

(e.g. Jing & Suto 2002), with the asphericity of the potential increasing rapidly towards the center of the halo (Hayashi et al. 2006). Gas cooling tends to circularize the potential (e.g. Dubinski 1994; Kazantzidis et al. 2004), while subsequent mergers produce highly elongated remnants (e.g. Moore et al. 2004). Studies of weak gravitational lensing and X-ray observations of elliptical galaxies show that halos are significantly flattened, in fair agreement with results from numerical simulations (Hoekstra et al. 2004; Buote et al. 2002). Yet the coherence of tidal debris from the Sagittarius dwarf galaxy appears to indicate that the inner halo of the MW is nearly spherical and therefore in conflict with CDM predictions (Ibata et al. 2001; but see Helmi 2004).

In this paper, we study the kinematics of HVSs in the MW as a probe of the triaxiality of the Galactic halo. The outline is as follows. In § 2, we analyze the motion of HVSs in a flattened or triaxial gravitational potential. We provide a concise statistical estimator for the triaxiality of the Galactic halo potential through the measured angular momenta of HVSs. In § 3, we review the Galactic potential model to be used in our calculations. In § 4 we perform numerical simulations of the motion of HVSs to study their kinematics. Finally, in § 5, we summarize our conclusions.

2 MOTION OF HYPERVELOCITY STARS

Consider a star with position vector \vec{r} moving with velocity \vec{v} in a gravitational potential $\Phi = \Phi_{\text{sph}}(r) + \Phi_{\text{nsph}}(x, y, z)$, where Φ_{sph} and Φ_{nsph} are the spherically-symmetric and aspherical component of the potential, (x, y, z) are Cartesian coordinates, and $r = \sqrt{x^2 + y^2 + z^2}$. The rate of change of the specific angular momentum of the star, $\vec{J} = \vec{r} \times \vec{v}$, is equal to the torque,

$$d\vec{J}/dt = -\vec{r} \times \nabla\Phi = -\vec{r} \times \nabla\Phi_{\text{nsph}}, \quad (1)$$

and has components

$$\begin{cases} dJ_x/dt = 2yz (\partial\Phi_{\text{nsph}}/\partial y^2 - \partial\Phi_{\text{nsph}}/\partial z^2), \\ dJ_y/dt = 2xz (\partial\Phi_{\text{nsph}}/\partial z^2 - \partial\Phi_{\text{nsph}}/\partial x^2), \\ dJ_z/dt = 2xy (\partial\Phi_{\text{nsph}}/\partial x^2 - \partial\Phi_{\text{nsph}}/\partial y^2). \end{cases} \quad (2)$$

It is convenient to change from Cartesian to spherical coordinates, $(x, y, z) = (r \sin \theta \cos \phi, r \sin \theta \sin \phi, r \cos \theta)$, and combine the above equations to yield

$$\frac{dJ_x/dt}{\sin \theta \sin \phi \cos \theta} + \frac{dJ_y/dt}{\sin \theta \cos \phi \cos \theta} + \frac{dJ_z/dt}{\sin^2 \theta \cos \phi \sin \phi} = 0. \quad (3)$$

From the definition of angular momentum it is also easy to derive

$$\mathcal{J}_x + \mathcal{J}_y + \mathcal{J}_z = 0, \quad (4)$$

where

$$\begin{cases} \mathcal{J}_x \equiv J_x / (\sin \theta \sin \phi \cos \theta), \\ \mathcal{J}_y \equiv J_y / (\sin \theta \cos \phi \cos \theta), \\ \mathcal{J}_z \equiv J_z / (\sin^2 \theta \cos \phi \sin \phi) \end{cases} \quad (5)$$

are determined directly from the position and velocity of the star. Note that equations (3) and (4) are rotationally invariant, that is, they do not change when arbitrary rotations are applied to their arguments. Below we apply the above analysis to the motion of stars in two simple cases of non-spherical potentials.

- If the non-spherical component of the gravitational potential is axisymmetric about the plane $z = 0$,

$$\Phi_{\text{nsph}} = \Phi_{\text{nsph}}(R = \sqrt{x^2 + y^2}, z), \quad (6)$$

then $\partial\Phi_{\text{nsph}}(R, z)/\partial x^2 = \partial\Phi_{\text{nsph}}(R, z)/\partial y^2$, and J_z is conserved. Stars ejected from the Galactic center on radial orbits move in a plane with

$$\mathcal{J}_x = -\mathcal{J}_y, \quad \mathcal{J}_z = 0. \quad (7)$$

- If the non-spherical component of the potential is triaxial,

$$\Phi_{\text{nsph}} = \Phi_{\text{nsph}}(x^2 + y^2/p^2 + z^2/q^2), \quad (8)$$

then a triaxiality parameter can be defined as

$$T \equiv \frac{p^{-2} - 1}{q^{-2} - 1}. \quad (9)$$

If $p = q = 1$, the potential reduces to the spherical case. If $p = 1$ and $q \neq 1$ ($T = 0$), $q = 1$ and $p \neq 1$, or $p = q \neq 1$ ($T = 1$), the potential is axisymmetric. If $q < p < 1$, the triaxiality parameter is $0 < T < 1$. In a triaxial potential, equation (2) can be written as

$$\frac{dJ_z/dt}{\sin^2 \theta \cos \phi \sin \phi} = -T \frac{dJ_y/dt}{\sin \theta \cos \phi \cos \theta}. \quad (10)$$

For HVSs moving away from the Galactic center on radial orbits, the deviation of their trajectory from the initial ejection direction, $(\delta\theta, \delta\phi)$, is small. Replacing the angles (θ, ϕ) in equation (10) with $(\theta \pm \delta\theta, \phi \pm \delta\phi)$ and integrating yields

$$T = -\frac{\mathcal{J}_z}{\mathcal{J}_y} \left[1 \mp \frac{2\delta\theta}{\sin(2\theta)} \mp \frac{\delta\phi}{\tan \phi} + \frac{\delta^2\theta}{\sin^2 \theta} + \frac{\delta^2\phi}{\sin^2 \phi} + \frac{2\delta\theta\delta\phi}{\sin(2\theta)\tan \phi} + \dots \right], \quad (11)$$

where the sin and cos arguments have been kept constant in the integration. The term in parenthesis specifies the maximum systematic error on the triaxiality estimator $T = -\mathcal{J}_z/\mathcal{J}_y$, and numerical calculations (see § 4 below) of the motion of HVSs in a triaxial potential show that the typical error on T is actually smaller. For a sample of N HVSs we can use equation (11) to construct a statistical estimator of triaxiality as

$$\bar{T} = \frac{\sum_{i=1}^N T_i}{\sum_{i=1}^N \sigma_{T_i}^2} / \frac{\sum_{i=1}^N 1}{\sum_{i=1}^N \sigma_{T_i}^2}, \quad (12)$$

with standard deviation

$$\sigma_{\bar{T}} = \left(\sum_{i=1}^N \frac{1}{\sigma_{T_i}^2} \right)^{-1/2}. \quad (13)$$

Here

$$T_i \equiv -\frac{\mathcal{J}_{z,i}}{\mathcal{J}_{y,i}} = -\frac{J_{z,i} \cos \theta_i}{J_{y,i} \sin \theta_i \sin \phi_i}, \quad (14)$$

and σ_{T_i} is its error. Note that the parameters T_i are fully determined by the instantaneous positions and velocity vectors of the HVSs in the sample, and that, while the ratio $-\mathcal{J}_{z,i}/\mathcal{J}_{x,i}$ can also be used to estimate the triaxiality $(1-p^{-2})/(q^{-2}-p^{-2})$, this does not provide any independent information since it can be trivially derived from $\mathcal{J}_{z,i}/\mathcal{J}_{y,i}$ using equation (4).

In the following we set the z -axis of the triaxial potential to be normal to the Galactic disk plane, and denote with η_0 the angle measured counter-clockwise from a reference direction (e.g. the line from the Galactic center to the Sun) to the x -axis of the potential. The ratio $-\mathcal{J}'_{z,i}/\mathcal{J}'_{y,i}$ in a frame forming an angle η with the reference direction can be written as

$$-\frac{\mathcal{J}'_{z,i}}{\mathcal{J}'_{y,i}} = \frac{\frac{1}{p^2} - 1}{\left(\frac{1}{q^2} - 1\right)A - \left(\frac{1}{p^2} - 1\right)B}, \quad (15)$$

where

$$A = \frac{\sin(2\phi'_i)}{\sin[2(\eta - \eta_0 + \phi'_i)]}, \quad B = \frac{\sin(\eta - \eta_0) \sin \phi'_i}{\cos(\eta - \eta_0 + \phi'_i)}. \quad (16)$$

If $\eta \neq \eta_0$, the values $-\mathcal{J}'_{z,i}/\mathcal{J}'_{y,i}$ may spread out over a large range due to the different angles ϕ'_i in the sample. The angle η_0 can be estimated by minimizing the weighted variance of $T'_i \equiv -\mathcal{J}'_{z,i}/\mathcal{J}'_{y,i}$:

$$\sum_{i=1}^N \left(\frac{T'_i - \bar{T}'}{\sigma_{T'_i}^2 / \sigma_{\bar{T}'}^2} \right)^2, \quad (17)$$

where $\sigma_{T'_i}$ is the error of T'_i and the values of \bar{T}' and $\sigma_{\bar{T}'}$ are obtained from equations (12) and (13).

3 GALACTIC GRAVITATIONAL POTENTIAL

We use here a four-component model for the gravitational potential of the Milky Way, $\Phi = \Phi_{\text{BH}} + \Phi_{\text{bulge}} + \Phi_{\text{disk}} + \Phi_{\text{halo}}$, where (cf. Gnedin et al. 2005):

- Φ_{BH} is the contribution of Sgr A*,

$$\Phi_{\text{BH}} = -\frac{GM_{\text{BH}}}{r}, \quad (18)$$

with mass $M_{\text{BH}} \simeq 3.6 \times 10^6 M_{\odot}$ (Ghez et al. 2005; Eisenhauer et al. 2005). The radius of influence of Sgr A* is $GM_{\text{BH}}/\sigma_c^2 \simeq 1.6 \text{ pc}$ ($M_{\text{BH}}/3.6 \times 10^6 M_{\odot})(100 \text{ km s}^{-1}/\sigma_c)^2$, where σ_c is the one-dimensional stellar velocity dispersion in the Galactic center.

- Φ_{bulge} is the contribution of the spherical bulge (Hernquist 1990),

$$\Phi_{\text{bulge}} = -\frac{GM_{\text{bulge}}}{r + a_{\text{bulge}}}, \quad (19)$$

with mass $M_{\text{bulge}} = 10^{10} M_{\odot}$ and core radius $a_{\text{bulge}} = 0.6 \text{ kpc}$. As both the bulge mass and size are small compared to those of the Galactic disk and halo, a slight deviation of the bulge from sphericity will not have a significant effect on the change of angular momentum of HVSs in the halo.

- Φ_{disk} is the contribution of the axisymmetric disk (Miyamoto & Nagai 1975),

$$\Phi_{\text{disk}}(R, z) = -\frac{GM_{\text{disk}}}{\sqrt{R^2 + \left(a_{\text{disk}} + \sqrt{z^2 + b_{\text{disk}}^2}\right)^2}}, \quad (20)$$

with mass $M_{\text{disk}} = 4 \times 10^{10} M_{\odot}$, scale length $a_{\text{disk}} = 5 \text{ kpc}$, and scale height $b_{\text{disk}} = 0.3 \text{ kpc}$.

- Φ_{halo} is the contribution of the triaxial dark matter

halo,

$$\Phi_{\text{halo}}(x, y, z) = \Phi_{\text{NFW}}(r^t), \quad (21)$$

$$r^t = p^{1/3} q^{1/3} \left(x^2 + \frac{y^2}{p^2} + \frac{z^2}{q^2} \right)^{1/2}, \quad (22)$$

$$\Phi_{\text{NFW}}(r^t) = -\frac{GM_{200} \ln(1 + r^t/r_s)}{r_s f(c) r^t/r_s}. \quad (23)$$

Here $c \equiv r_{200}/r_s$ is the halo concentration parameter, r_{200} the radius within which the enclosed average density is 200 times the mean matter density, r_s the scale radius, and $f(c) = \ln(1 + c) - c/(1 + c)$. This generalization of an NFW (Navarro et al. 1996) model ensures that the spherically-averaged potential of the triaxial halo is similar to that of a spherical halo with the same mass M_{200} and scale radius (Hayashi et al. 2006). We choose the following parameters for the Milky Way halo: $c = 15$, $r_{200} = 389 \text{ kpc}$, $M_{200} = 1.8 \times 10^{12} M_{\odot}$ (e.g. Diemand et al. 2007), and assume that the z -axis of the halo and disk potentials coincide. We also assume, for simplicity, that the asphericity of the potential is constant with radius r , and set $p = 0.8$ and $q = 0.7$ in the calculations below.

CDM halos are not smooth but have a wealth of substructure on all resolved mass scales (e.g. Moore et al. 1999; Klypin et al. 1999). The assumption made above of a smooth gravitational potential neglects the deflection of HVS trajectories by halo substructure. A star with velocity v passing within a distance r_* from a subhalo of mass M_{sub} will change its velocity by an amount $\delta v = 2GM_{\text{sub}}/(vr_*)$. The mass function of substructure in a Milky Way-sized halo can be described as $N(> M_{\text{sub}}) = 6.4 \times 10^{-3} (M_{200}/M_{\text{sub}})$ in the subhalo mass range $10^6 M_{\odot} < M_{\text{sub}} < f_{\text{max}} M_{200}$ (Diemand et al. 2007), with $f_{\text{max}} = 0.01$. The probability that a HVS ejected from the Galactic center is subject to a velocity deflection $> \delta v$ can then be estimated as

$$\begin{aligned} P(> \delta v) &= \frac{3}{4} \int \frac{r_*^2}{r_{200}^2} \frac{dN}{dM_{\text{sub}}} dM_{\text{sub}} \\ &\sim 0.08 \left(\frac{f_{\text{max}}}{0.01} \right) \left(\frac{V_c}{140 \text{ km s}^{-1}} \right)^4 \times \\ &\quad \left(\frac{10^3 \text{ km s}^{-1}}{v} \right)^2 \left(\frac{1 \text{ km s}^{-1}}{\delta v} \right)^2, \end{aligned} \quad (24)$$

where $V_c \equiv (GM_{200}/r_{200})^{1/2}$ is the halo circular velocity. This probability is quite low so that a smooth potential is a good assumption in this work.

4 NUMERICAL CALCULATIONS

In this section we perform numerical calculations of the motion of HVSs in the MW gravitational potential.

4.1 Initial conditions

According to the study of Yu & Tremaine (2003), three-body interactions between ambient stars and a BH pair (where the secondary BH may be an IMBH inspiralling towards Sgr A*; e.g., Baumgardt et al. 2006) expel HVSs ($v > 10^3 \text{ km s}^{-1}$) at a rate that can be as large as $\sim 10^{-4} \text{ yr}^{-1}$ (for a binary with semimajor axis $0.5 \times 10^{-3} \text{ pc}$ and mass

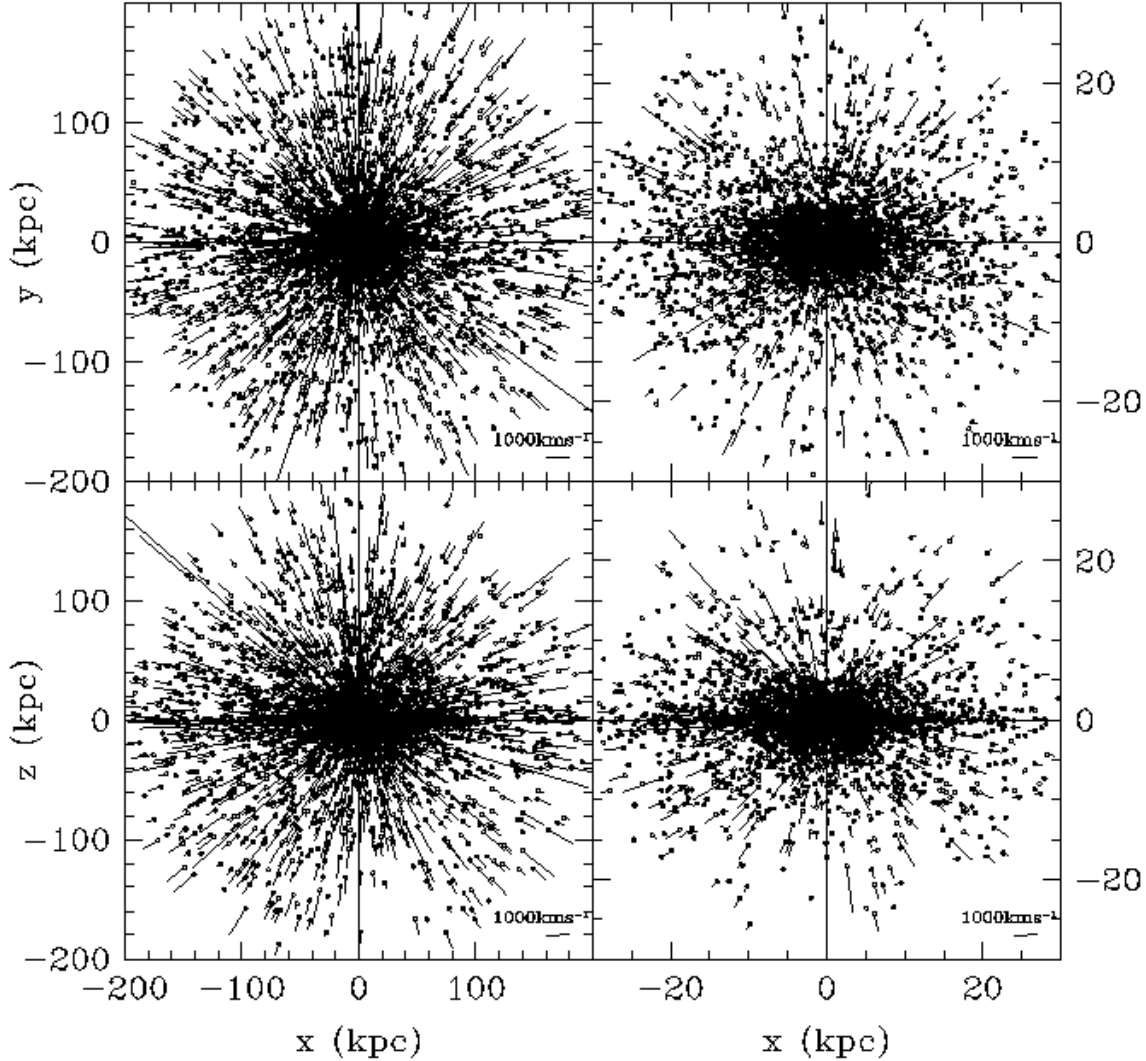


Figure 1. Present-day spatial distribution and velocity vectors of HVSs ejected by a binary BH at the Galactic center. The length of each vector is proportional to speed. Ten thousand HVSs were generated at a constant rate in the past 10^9 yr, with a velocity and spatial distribution obtained from the three-body scattering experiments of Sesana et al. (2006). The binary has a mass $3.6 \times 10^6 M_\odot$, mass ratio of 1/81, orbital semimajor axis equal to $0.1a_h$, and eccentricity 0.3, and orbits in the (x, y) plane. The reference axes are set along the (x, y, z) -axes of the triaxial halo potential in eq. (22).

ratio of 0.01). Tidal break-up of binary stars (“Hills’ mechanism”) ejects HVSs at a rate $\sim 10^{-5}(\eta/0.1) \text{ yr}^{-1}$, where η is the fraction of stars in binaries with semimajor axis $\lesssim 0.3$ AU. Close encounters of two single stars in the vicinity of Sgr A* may also produce HVSs but at the negligible rate of 10^{-11} yr^{-1} . Different ejection mechanisms give origin to different spatial and velocity distributions of HVSs. While Hills’ mechanism predict HVSs to be expelled isotropically at an approximately constant rate, in models involving a BH pair HVSs are ejected preferentially within the orbital plane of the binary in a short burst lasting a few Myr (Zier & Biermann 2001; Levin 2006; Sesana et al. 2006, 2007). In the latter case the degree of anisotropy depends on binary separation, the mass ratio, and the orbital eccentricity of the BH binary.

For illustrative purposes, we assume in this paper that HVSs are ejected from the Galactic center by the BH bi-

nary mechanism. We use the stellar spatial and velocity distributions derived from the scattering experiments of Sesana et al. (2006) for a binary with mass ratio $M_2/M_1 = 1/81$, semimajor axis $a = 0.1 a_h$, and eccentricity $e = 0.3$. The binary orbit is in the Galactic disk plane, and the velocity of the lighter hole at pericenter is directed along $\phi = 3\pi/2$. The “hardening” radius a_h is defined as (Quinlan 1996)

$$a_h \equiv \frac{GM_2}{4\sigma_c^2} \simeq 0.39 \text{ pc} \left(\frac{M_2}{M_1} \right) \left(\frac{M_1}{3.6 \times 10^6 M_\odot} \right) \left(\frac{100 \text{ km s}^{-1}}{\sigma_c} \right)^2 \quad (25)$$

When $a > a_h$, the binary separation decreases both by dynamical friction and three-body interactions with low-angular momentum stars passing in its immediate vicin-

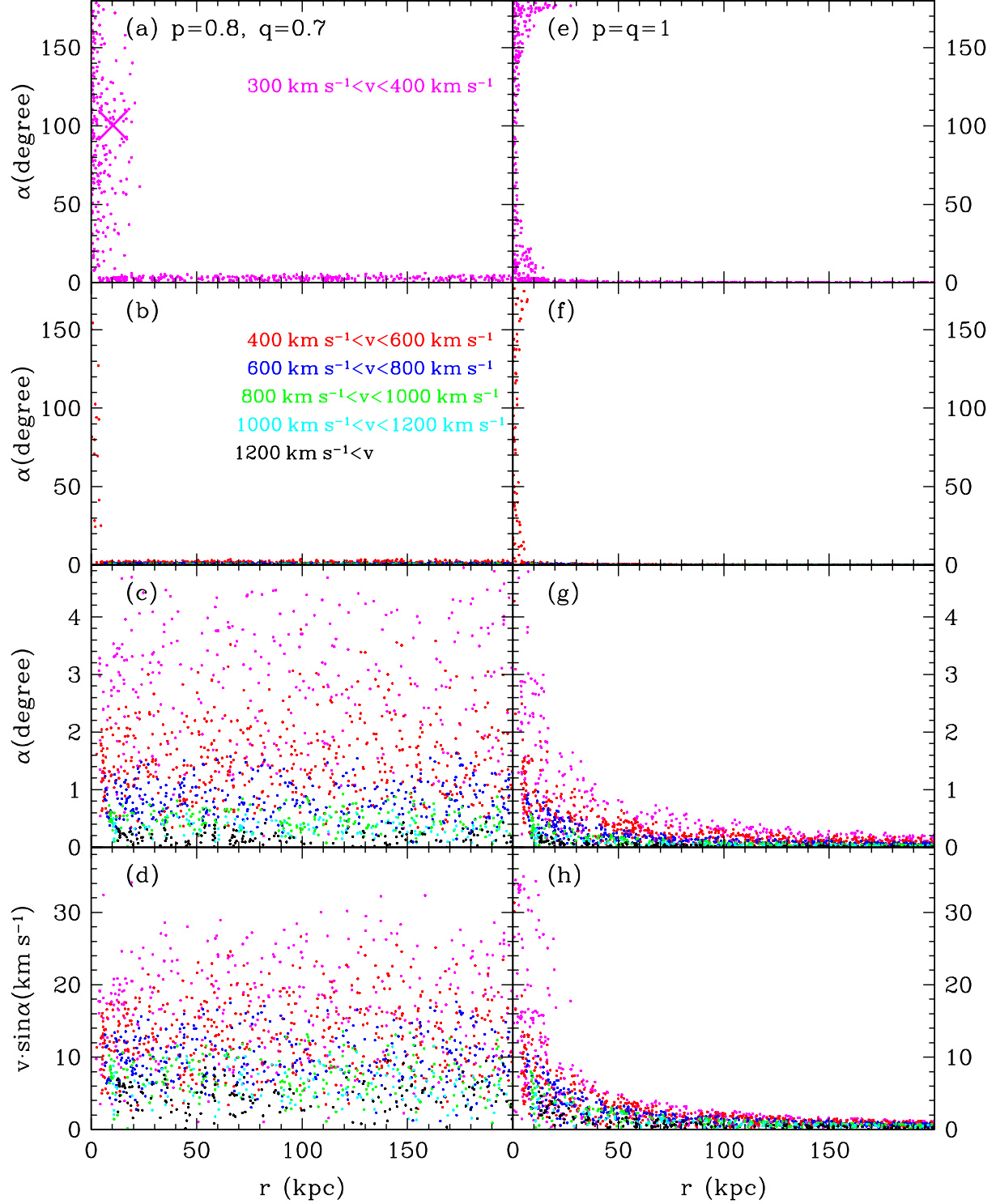


Figure 2. Panels (a)–(c): Deflection angle $\alpha = \arcsin(|\vec{r} \times \vec{v}|/rv)$ between velocity and position vectors for all HVSS plotted in Fig. 1, as a function of Galactocentric distance r . The panels show different velocity ranges or different scales in α . Panel (d): transverse velocity in the Galactocentric frame versus distance r for all stars shown in Panel (c). Panels (a)–(d): triaxial halo potential with $p = 0.8$ and $q = 0.7$ (see eq. 22). Panels (e)–(h): spherical halo potential with $p = q = 1$. Different colors depict different velocity ranges: 300–400 km s^{-1} (magenta), 400–600 km s^{-1} (red), 600–800 km s^{-1} (blue), 800–1000 km s^{-1} (green), 1000–1200 km s^{-1} (cyan), > 1200 km s^{-1} (black). HVSS with angles between 5° and 180° in Panels (a), (b), (e) and (f) are bound stars with significantly bent orbits, and their detailed α distribution depends on halo triaxiality. Stars with small deflections ($\alpha \lesssim 5^\circ$) are either unbound (and have distances $\gtrsim 10$ kpc) or are in the initial phases of their orbital period (and are closer to the Galactic center, see also Fig. 5). The large cross in Panel (a) flags the locus of the bound star whose orbit is shown in Fig. 3.

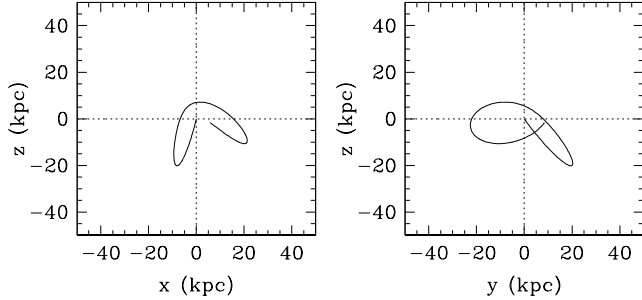


Figure 3. The bound orbit of a simulated HVS ejected from the Galactic center. The orbit is significantly bent, rather than radial as expected in a spherical potential. The star’s travel time 820 Myr, and its present-day velocity and Galactocentric distance are 300 km s^{-1} and 10 kpc, respectively.

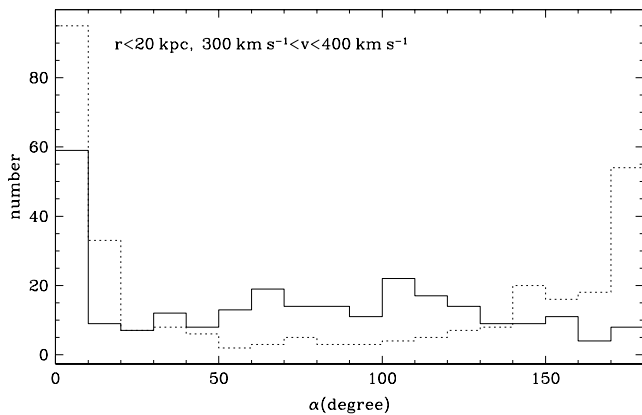


Figure 4. Histogram of the deflection angle distribution of all stars shown in Fig. 2(a) (*solid line*) and (e) (*dotted line*) with $r < 20 \text{ kpc}$ and $300 \text{ km s}^{-1} < v < 400 \text{ km s}^{-1}$. The bound stars are clustered around 0° and 180° in a spherical halo potential (*dotted line*), while their distribution is spread uniformly over the range 10° – 180° in a triaxial halo potential (*solid line*).

ity. After the binary becomes “hard” ($a < a_h$), the bound pair loses orbital energy mainly through three-body interactions until gravitational radiation takes over (Begelman, Blandford & Rees 1980; Yu 2002). The ejection speed of the stars at infinity spans a range with r.m.s. $\sim 7 \times 10^2 \text{ km s}^{-1} (M_2/0.01 M_{\text{BH}})^{1/2} (10^{-3} \text{ pc}/a)^{1/2} (M_{\text{BH}}/3.6 \times 10^6 M_\odot)^{1/2}$ (see eq. 33 in Yu & Tremaine 2003). In the calculations below, we assume 10^4 HVSs are ejected from the Galactic center at a constant rate over the last 10^9 years, and ignore for simplicity the orbital evolution of the binary during such timescale. Different stars move independently in the Galactic potential. A fourth-order Runge-Kutta method with adaptive stepsize control is used to solve the differential equations of the motion of the stars. Note that the adopted mass ratio and semimajor axis are within the allowed parameter space for a BH pair at the Galactic center (see Fig. 2 in Yu & Tremaine 2003).

4.2 Results

We use the initial conditions described above and numerically integrate the orbits of HVSs in the Galactic potential.

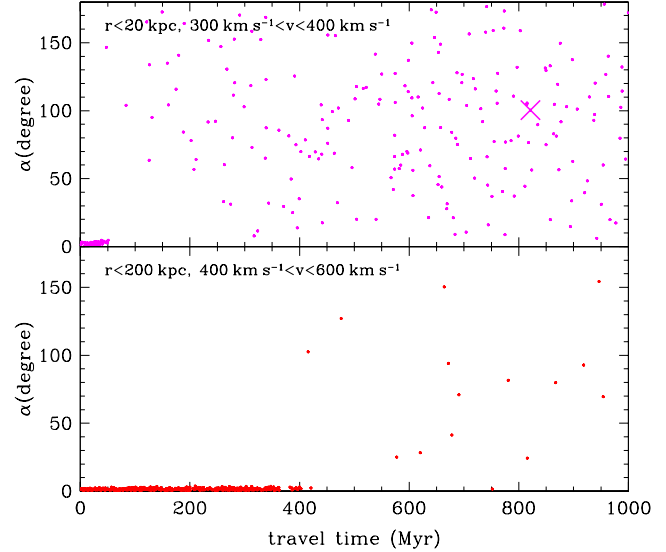


Figure 5. Deflection angle versus travel time from the Galactic center. *Top panel:* all stars shown in Fig. 2(a) with $r < 50 \text{ kpc}$ and $300 \text{ km s}^{-1} < v < 400 \text{ km s}^{-1}$. *Bottom panel:* all stars shown in Fig. 2(b) with $r < 200 \text{ kpc}$ and $400 \text{ km s}^{-1} < v < 600 \text{ km s}^{-1}$. HVSs with short travel times, $\lesssim 50 \text{ Myr}$ (*top*) and $\lesssim 400 \text{ Myr}$ (*bottom*) have α angles smaller than 5° . The large cross in the top panel flags the locus of the bound star whose orbit is shown in Fig. 3.

Figures 1 and 2 show maps of stellar position and velocity vectors at the present time and their deflection angles $\alpha = \arcsin(|\vec{r} \times \vec{v}|/rv)$. For HVSs with $v \gtrsim 600 \text{ km s}^{-1}$, deviations are quite small, $\alpha \lesssim 5^\circ$, at all distances within 200 kpc. Lower velocity stars at small distances can instead be bound, and their deflection angles extend to 180° . Many of the stars with $300 \text{ km s}^{-1} \lesssim v \lesssim 400 \text{ km s}^{-1}$ and $r \lesssim 20 \text{ kpc}$ in Figure 2(a) follow bound trajectories, while no stars in this velocity range have substantial deviation angles at large Galactocentric distances. One example of a bound orbit is shown in Figure 3, where the trajectory has been significantly bent by the triaxial halo and the flattened disk potentials, and the star does not return to the Galactic center. Note that bound stars with $v > 400 \text{ km s}^{-1}$ and large α ’s are typically observed at smaller distances ($r \lesssim 10 \text{ kpc}$) than bound stars of lower velocities. This is because a larger ejection speed from the Galactic center is needed to maintain a high velocity at large distances, and such stars may then have either escaped from the halo or not have had sufficient time to come back and show a significant bend in their orbits. (For reference, the local escape speed is about $500 - 600 \text{ km s}^{-1}$, Smith et al. 2006.) We find that 60% of the stars with $v > 300 \text{ km s}^{-1}$ at $r < 20 \text{ kpc}$ have velocities $v < 400 \text{ km s}^{-1}$, and 20% of the stars with $v > 300 \text{ km s}^{-1}$ at $r < 10 \text{ kpc}$ have velocities $v < 600 \text{ km s}^{-1}$.

Figure 5 shows that bound stars with large deflection angles ($5^\circ \lesssim \alpha \lesssim 180^\circ$) have generally traveled a long time after ejection ($\gtrsim 50 \text{ Myr}$ for $r \lesssim 20 \text{ kpc}$), and many of them have experienced at least one orbital period (Fig. 3). HVSs with small deflections ($\alpha \lesssim 5^\circ$) have instead a short travel time and are generally on the initial phases of their first orbital periods (see the concentration of the stars at the left bottom of the panels in Figure 5). The

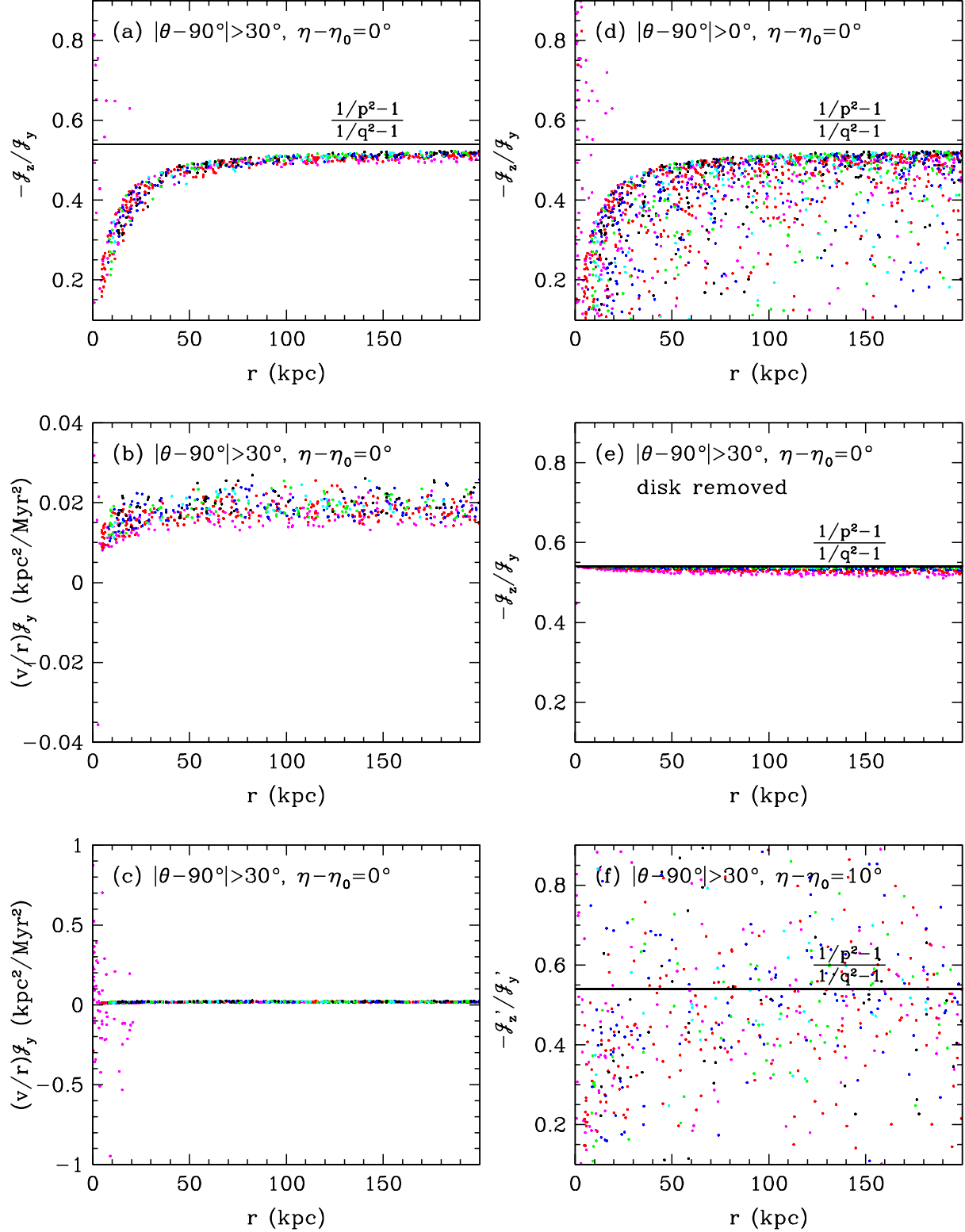


Figure 6. The variables $-\mathcal{J}_z/\mathcal{J}_y$ and $(v/r)\mathcal{J}_y$ versus Galactocentric distances r for all HVSs far from the plane of the disk, $|\theta - 90^\circ| < 30^\circ$. Stars near the plane are included only in Panel (d). Different colors represent different velocity ranges as in Fig. 2. Panel (c) shows \mathcal{J}_y on a different scale than Panel (b), and the scattered magenta dots are bound stars with significantly bent orbits. Panel (e) shows the effect of removing the disk potential from the calculation. Panel (f) shows the results in a reference frame with $\eta - \eta_0 = 10^\circ$, different from the triaxial frame of the halo potential. The solid line represents the triaxiality of the halo potential $T = 0.54$ (with $p = 0.8$ and $q = 0.7$ in eq. 9) assumed in the calculation.

transverse velocities (in the Galactocentric frame) of stars with $v > 300 \text{ km s}^{-1}$ are typically higher than 3 km s^{-1} , and can be up to 30 km s^{-1} (hundreds of km s^{-1}) for unbound (bound) HVSs. Note that 3 km s^{-1} corresponds at a distance of 100 kpc to a proper motion of $20 \mu\text{as}$ in three years, which can be resolved by the next generation of astrometric surveys like GAIA. According to our calculations most HVSs would have transverse velocities $\gtrsim 3 \text{ km s}^{-1}$ even in the case of a weakly triaxial halo with $(p, q) = (0.95, 0.9)$: these transverse velocities are larger than those associated with the bending of stellar trajectories caused by the axisymmetric disk (see Fig. 2h).

A comparison between Figures 2(e)–(g) and 2(a)–(c) shows that the distribution of deflection angles versus distance is different for trajectories in a spherical rather than triaxial halo. In Figure 2(e) and (f), the α angles of bound stars are clustered around 0° and 180° because their orbits are highly eccentric with little bending (see also Fig. 4). By contrast, in Figure 2(a) and (b) the deflection angles of bound stars lies at intermediate values. This difference can be used as an indicator of the triaxiality of the MW dark matter halo.

Figure 6(a)–(c) depicts the values of $-\mathcal{J}_z/\mathcal{J}_y$ and $(v/r)\mathcal{J}_y$ versus distance of all the HVSs plotted in Figure 1 having $v > 300 \text{ km s}^{-1}$ and far from the plane of the disk, i.e. with $|\theta - 90^\circ| > 30^\circ$. Figure 6(d) shows all stars with θ in the range 0° – 180° . As seen in Figure 6(a), the ratio $-\mathcal{J}_z/\mathcal{J}_y$ at large distances ($r \gtrsim 100 \text{ kpc}$) is close to the triaxiality of the halo potential ($T = 0.54$, *solid line*) assumed in our calculations, with only a small scatter. The scatter is larger in the quantity $(v/r)\mathcal{J}_y$ plotted in Figure 6(b). The slight offset ($\lesssim 10\%$) of the stellar dots from the solid line is partly due to the disk potential that causes an additional bending of stellar trajectories towards the disk plane, increasing $|\mathcal{J}_y|$ without changing \mathcal{J}_z (see the Appendix for details about the correction of such offset owing to the Galactic disk). As shown in Figure 6(e), HVSs become better tracers of triaxiality after removing the disk potential from our calculations. The higher the velocities, the smaller the offset. The curvature of the ratio $-\mathcal{J}_z/\mathcal{J}_y$ towards smaller values at small distances is also an effect of the disk. The ratio $-\mathcal{J}_z/\mathcal{J}_y$ for stars close to disk plane is not a good approximation of halo triaxiality even at large distances (see Fig. 6d). We plot the values of \mathcal{J}_z versus \mathcal{J}_y in Figure 7, where Panel (a) shows stars with $|\theta - 90^\circ| < 30^\circ$, and Panel (b) stars with θ in the full range 0° – 180° . The effect of the disk potential can be seen in the spreading of the stellar dots from the solid line $\mathcal{J}_z = -T\mathcal{J}_y$ to the dashed line $\mathcal{J}_z = 0$. Note that the scatter in the ratio $-\mathcal{J}_z'/\mathcal{J}_y'$ increases significantly if the reference frame is different from the frame of the triaxial halo potential (Fig. 6f).

5 SUMMARY

We have studied the unique kinematics of HVSs ejected from the Galactic center with almost zero initial specific angular momentum. HVSs can travel in the Galactic halo on either bound or unbound orbits, and their spatial and velocity distribution at large Galactocentric distances ($r \gtrsim 50 \text{ kpc}$) contain information on the asphericity of the halo gravitational potential. We have proposed an estimator of the triaxiality

of the Galactic dark matter halo that is determined solely by instantaneous position and velocity vectors of HVSs, is independent of the details of the ejection mechanism, and does not require an accurate knowledge of halo mass. Future astrometric and deep wide-field surveys of HVSs should detect significant numbers of HVSs, which could be used to determine the triaxiality of the MW halo by applying the method proposed in this paper.

The new class of possibly bound HVSs with velocities $+275 < v_{\text{rf}} < +450 \text{ km s}^{-1}$ recently observed by Brown et al. (2007) has Galactocentric distances in the range 30–60 kpc or 10–20 kpc depending on whether they are main-sequence or blue horizontal branch stars. In the first case (main-sequence stars at large distances), they have a lifetime of $\lesssim 100 \text{ Myr}$ and are, according to Figure 5, on the initial phases of their first orbital periods. Their deflection angles are expected to be rather small, supporting the fact that a significant excess of B-type stars is observed only at large positive velocities (Brown et al. 2007). If bound HVSs are blue horizontal branch stars instead at smaller distances, the travel time of the stars can be much longer than 50 Myr as at the ejection moment the stars may not necessarily be blue horizontal branch stars but at some pre-blue-horizontal-branch stage. Such stars may have experienced at least one orbital period, and many of them should be returning to the Galactic center or their orbits should have been significantly bent by the asymmetric Galactic potential (Fig. 5). This scenario appear unlikely since it does not agree with the observed positive radial velocities.

It is interesting at this stage to provide an example of a statistical estimate of halo triaxiality from a mock sample. Let us assign a measurement error of $\sigma_a = 3 \text{ km s}^{-1}$ ($a = x, y, z$) to the one-dimensional velocities of all stars in Figure 6(a) having $v > 300 \text{ km s}^{-1}$, $|\theta - 90^\circ| > 30^\circ$, and $55 \text{ kpc} < r < 200 \text{ kpc}$ (our error analysis assumes that the distances to HVSs are known to within ten percent). We have simulated the observed velocities of such a sample, and plot in the top panel of Figure 8 the values of T_i and σ_{T_i} derived for each HVS. Using equations (12) and (13), we obtain $\bar{T} = 0.50$ and $\sigma_{\bar{T}} = 0.02$. For $\sigma_a = 5 \text{ km s}^{-1}$, we obtain $\bar{T} = 0.50$ and $\sigma_{\bar{T}} = 0.03$. These errors are comparable with the systematic error caused by the flattened disk (see the slight offset of dots from the solid line in Fig. 6a). We have tried different values of the gravitational potential parameters (p, q) in the calculations, and found that the estimated value of \bar{T} is always consistent with the assumed halo triaxiality (see middle and bottom panels in Fig. 8).

If the x -axis of the halo potential form an angle η_0 (measured counter-clockwise) with the reference axis of the observations, then (as seen from Fig. 9) the minimum variance of $\mathcal{J}'_{z,i}/\mathcal{J}'_{y,i}$ in a set of simulated samples each in a frame at angle η from the observational reference axis (see eq. 17) occurs for $\eta = \eta_0$. Our calculations show that an error of 5° in the estimate of η_0 may cause an error of 2% in the estimate of \bar{T} .

Note that the axis ratios (p, q) of the halo potential are degenerate in the defined triaxiality parameter (eq. 9). After determining T , the values of (p, q) could be also obtained by using any value of $(\mathcal{J}_x, \mathcal{J}_y, \mathcal{J}_z)$ (e.g., see Fig. 6b), but the modeling would be sensitive to halo mass and the shape of halo potential used (see also the determination of axis ratios in Gnedin et al. 2005 by tracing back HVS orbits).

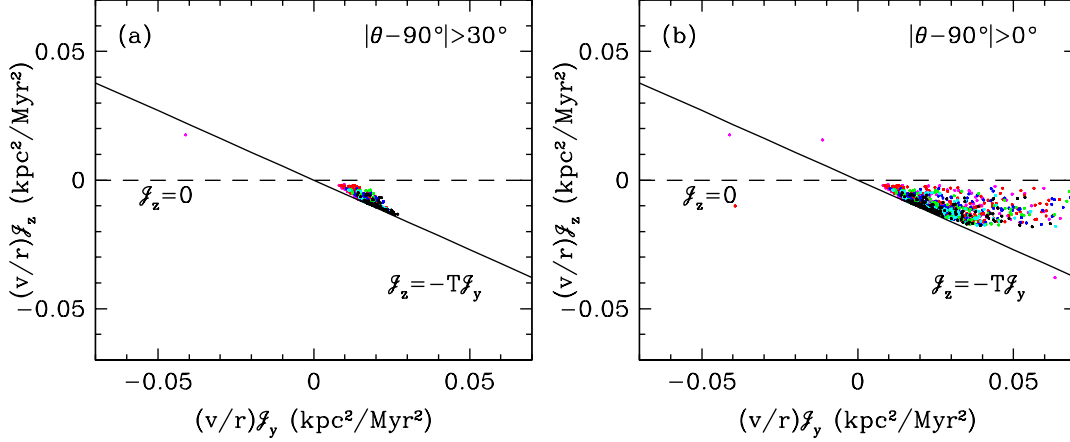


Figure 7. The variable $(v/r)J_z$ versus $(v/r)J_y$. The solid and dashed lines correspond to $J_z = -TJ_y$ and $J_z = 0$ (see eq. 7), respectively. The stars are those shown in Fig. 6. Panel (a) includes only stars far from the plane of the disk, $|\theta - 90^\circ| > 30^\circ$, while Panel (b) includes all stars. The effect of the disk potential can be gauged from the spread of the stellar dots from the solid line to the dashed line in Panel (b). The magenta and red dots scattered above the dashed line or below the solid line represent bound stars with bent orbits.

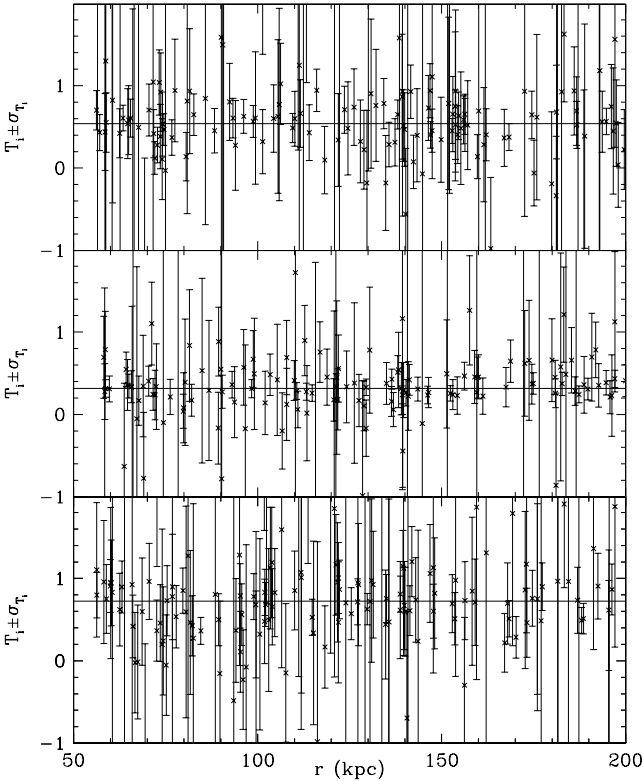


Figure 8. Simulated triaxiality parameters and their errors from a mock sample of HVSS with $v > 300 \text{ km s}^{-1}$, $|\theta - 90^\circ| > 30^\circ$, and $55 \text{ kpc} < r < 200 \text{ kpc}$. An observational error of 3 km s^{-1} is assumed for in “measured” one-dimensional velocity. From top to bottom, the values of (p, q) used in the calculations are $(0.8, 0.7)$, $(0.8, 0.6)$, and $(0.8, 0.75)$, corresponding to a triaxiality $T=0.54$, 0.32 , and 0.72 , respectively (*horizontal lines*). A statistical analysis of the sample using eqs. (12) and (13) yields $(\bar{T}, \sigma_{\bar{T}})=(0.50, 0.02)$, $(0.31, 0.01)$, and $(0.64, 0.02)$, respectively. For clarity, only 1/3 of the sample points are drawn in the figure.

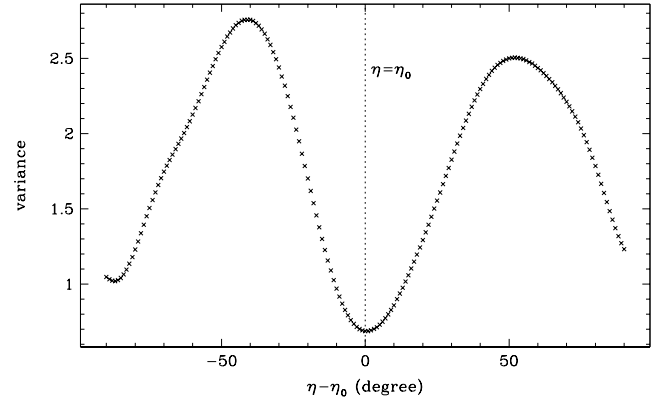


Figure 9. Variance of the triaxiality parameter T' of the simulated sample (top panel in Fig. 8) in different reference frames as a function of $\eta - \eta_0$. Here η_0 is the angle measured counter-clockwise from a reference center (e.g. the line from the Galactic center to the Sun) to the x -axis of the halo potential, and η is the angle formed by the observational frame with the reference direction. The variance has a minimum at $\eta - \eta_0 = 0^\circ$.

Finally, it is possible that a few HVSS in the halo may be produced by the interactions of stars with an IMBH in satellite galaxies like the Large Magellanic Cloud (Edelmann et al. 2005; Gualandris & Portegies Zwart 2007), and that these would contaminate the sample ejected from the Galactic center. The ejection rates from the satellite dwarfs of the MW are expected to be much smaller than the rate from Sgr A*, however. Such “satellite” HVSS will also have much larger angular momenta in the Galactocentric rest-frame, and should be easily distinguishable from the Galactic center sample.

We have benefited from discussions with Francesco Haardt, Youjun Lu, and Scott Tremaine. We thank Alberto Sesana for providing the initial velocity and spatial distributions of HVSS ejected from a black hole binary. P.M. acknowledges financial support from NASA through grants NAG5-11513 and NNG04GK85G, and from the Alexander

von Humboldt Foundation. Q.Y. acknowledges initial support from NASA through Hubble Fellowship grant HST-HF-01169.01-A awarded by the Space Telescope Science Institute, which is operated by the Association of Universities for Research in Astronomy, Inc., for NASA, under contract NAS 5-26555.

APPENDIX A: CORRECTION OF THE EFFECT OF DISK POTENTIAL ON THE INFERRED HALO TRIAXIALITY

As shown in Figure 6(a), the triaxiality obtained through $T = -\mathcal{J}_z/\mathcal{J}_y$ has a small offset from the true halo triaxiality. Part of this offset comes from the effects of the flattened disk potential, and part from the fixing of (θ, ϕ) in the integration of equation (10). The offset due to the constant (θ, ϕ) assumption is smaller for stars of higher velocities, as seen in Figure 6(e) that shows the results after the disk potential was removed. Below we provide a method to correct the offset due to the Galactic disk. As in the determination of halo triaxiality proposed in this work, even for this correction it is not necessary to trace back the orbits of HVSs.

The contribution to the change in specific angular momentum due to the disk potential can be expressed as:

$$J_{y,\text{disk}} = \int_{r_{\text{ej}}}^{r_0} \frac{dJ_{y,\text{disk}}}{dt} \frac{dt}{dr} dr, \quad (\text{A1})$$

where

$$\frac{dJ_{y,\text{disk}}}{dt} = 2xz \left(\frac{\partial \Phi_{\text{disk}}}{\partial z^2} - \frac{\partial \Phi_{\text{disk}}}{\partial x^2} \right), \quad (\text{A2})$$

$$\frac{dt}{dr} = \frac{1}{v_r} \simeq \frac{1}{\sqrt{v_0^2 + 2\Phi(\vec{r}_0) - 2\Phi(\vec{r})}}, \quad (\text{A3})$$

r_{ej} is the initial distance of the HVS from the Galactic center at ejection, \vec{r}_0 and v_0 are the current position and velocity of the HVS, $r_0 = |\vec{r}_0|$, and v_r is its radial velocity at r . We can remove the effect of the disk potential from the variable \mathcal{J}_y by computing $\mathcal{J}_y - \mathcal{J}_{y,\text{disk}}$, where

$$\begin{aligned} \mathcal{J}_{y,\text{disk}} &= \frac{J_{y,\text{disk}}}{\sin \theta \cos \phi \cos \theta} \\ &= \int_{r_{\text{ej}}}^{r_0} \frac{GM_{\text{disk}}}{(r^2 + a_{\text{disk}}^2 + b_{\text{disk}}^2 + 2a_{\text{disk}}\sqrt{r^2 \cos^2 \theta + b_{\text{disk}}^2})^{3/2}} \\ &\quad \frac{a_{\text{disk}} r^2}{\sqrt{r^2 \cos^2 \theta + b_{\text{disk}}^2}} \frac{dr}{v_r}, \end{aligned} \quad (\text{A4})$$

and where equation (20) describing the disk potential has been used. The angles (θ, ϕ) are fixed in the integration to be present-day values. In addition to the disk potential, we also need to assume a halo potential to determine v_r , for which we may use the spherical part of the halo potential by setting $(p, q) = (1, 1)$. We have tested this correction and found that half of the offset to the true halo triaxiality can be corrected.

REFERENCES

Baumgardt, H., Gualandris, A., & Portegies Zwart, S. 2006, MNRAS, 372, 174

- Begelman, M. C., Blandford, R. D., & Rees, M. J. 1980, Nature, 287, 307
- Bromley, B. C., Kenyon, S. J., Geller, M. J., Barcikowski, E. B., Warren, R., & Kurtz, M. J. 2006, ApJ, 653, 1194
- Brown, W. R., Geller, M. J., Kenyon, S. J., & Kurtz, M. J. 2005, ApJ, 622, L33
- Brown, W. R., Geller, M. J., Kenyon, S. J., & Kurtz, M. J. 2006a, ApJ, 640, L35
- Brown, W. R., Geller, M. J., Kenyon, S. J., & Kurtz, M. J. 2006b, ApJ, 647, 303
- Brown, W. R., Geller, M. J., Kenyon, S. J., Kurtz, M. J., & Bromley, B. C. 2007, ApJ, in press (astro-ph/0701600)
- Buote, D. A., Jeltama, T. E., Canizares, C. R., & Garmire, G. P. 2002, ApJ, 577, 183
- Diemand, J., Kuhlen, M., & Madau, P. 2007, ApJ, 657, 262
- Dubinski, J. 1994, ApJ, 431, 617
- Edelmann, H., Napiwotzki, R., Heber, U., Christlieb, N., & Reimers, D. 2005, ApJ, 634, L181
- Eisenhauer, F., et al. 2005, ApJ, 628, 246
- Ghez, A. M., et al. 2005, ApJ, 620, 744
- Ginsburg, I., & Loeb, A. 2006, MNRAS, 368, 221
- Gnedin, O. Y., Gould, A., Miralda-Escudé, J., & Zentner, A. R. 2005, ApJ, 634, 344
- Gualandris, A., & Portegies Zwart, S. 2007, MNRAS, in press (astro-ph/0612673)
- Hayashi, E., Navarro, J. F., & Springel, V. 2006, MNRAS, in press (astro-ph/0612327)
- Helmi, A. 2004, MNRAS, 351, 643
- Hernquist, L. 1990, ApJ, 356, 359
- Hills, J. G. 1988, Nature, 331, 687
- Hirsch, H. A., Heber, U., O'Toole, S. J., & Bresolin, F. 2005, A&A, 444, L61
- Hoekstra, H., Yee, H. K. C., & Gladders, M. D. 2004, ApJ, 606, 67
- Ibata, R., Lewis, G. F., Irwin, M., Totten, E., & Quinn, T. 2001, ApJ, 551, 294
- Jing, Y. P., & Suto, Y. 2002, ApJ, 574, 538
- Kazantzidis, S., Kravtsov, A. V., Zentner, A. R., Allgood, B., Nagai, D., & Moore, B. 2004, ApJ, 611, L73
- Klypin, A. A., Kravtsov, A. V., Valenzuela, O., & Prada, F. 1999, ApJ, 630, L141
- Levin, Y. 2006, ApJ, 653, 1203
- Miyamoto, M., & Nagai, R. 1975, PASJ, 27, 533
- Moore, B., Ghigna, S., Governato, F., Lake, G., Quinn, T., Stadel, J., & Tozzi, P. 1999, ApJ, 524, L19
- Moore, B., Kazantzidis, S., Diemand, J., & Stadel, J. 2004, MNRAS, 354, 522
- Navarro, J. F., Frenk, C. S., & White, S. D. M., 1996, ApJ, 462, 563
- O'Leary, R. M., & Loeb, A. 2006, MNRAS, submitted (astro-ph/0609046)
- Quinlan, G. D. 1996, New Astron., 1, 35
- Sesana, A., Haardt, F., & Madau, P. 2006, ApJ, 651, 392
- Sesana, A., Haardt, F., & Madau, P. 2007, ApJ, in press (astro-ph/0612265)
- Smith, M. C., et al. 2006, MNRAS, submitted (astro-ph/0611671)
- Yu, Q. 2002, MNRAS, 331, 935
- Yu, Q., & Tremaine, S. 2003, ApJ, 599, 1129
- Zier, C., & Biermann, P. L. 2001, A&A, 377, 23